



Research paper

Combining radiative cooling and light trapping strategies for improved performance of PERC bifacial silicon solar cells



Unai Urdiruz^{a,b}, Iñigo Itoiz^c, Joaquín Sevilla^{d,e}, Angel Andueza^{d,e,*}

^a Dpto. Ingeniería, Universidad Pública de Navarra, 31006 Pamplona, Spain

^b Institute for Advanced Materials (INAMAT), Universidad Pública de Navarra, 31006 Pamplona, Spain

^c Solafam Ingeniería, 31006 Pamplona, Navarra, Spain

^d Dpto. Ing. Eléctrica, Electrónica y Comunicación, Universidad Pública de Navarra, 31006 Pamplona, Spain

^e Smart Cities Institute (SCI), Universidad Pública de Navarra, 31006 Pamplona, Spain

ARTICLE INFO

Article history:

Received 29 March 2023

Received in revised form 7 July 2023

Accepted 22 July 2023

Available online xxxx

Keywords:

Texturing

Radiative cooling

Light trapping

Bifacial solar cell

PERC

Antireflective

ABSTRACT

This work investigates the impact of combining light trapping and radiative cooling on bifacial solar panels. While several techniques have been proposed to enhance the efficiency of solar panels, their combination can lead to suboptimal results. By numerically evaluating the light absorption and thermal balance of different panel configurations, we found that each side of the bifacial solar cell can be textured independently with a cross-effect of less than 4%. However, our results also indicate that improving visible light trapping can increase infrared absorption, leading to a heating effect that may offset the benefits of radiative cooling. These findings highlight the importance of balancing the factors that influence solar panel efficiency and provide quantitative insights that guide the development of more effective solar energy systems.

© 2023 The Authors. Published by Elsevier Ltd. This is an open access article under the CC BY-NC-ND license (<http://creativecommons.org/licenses/by-nc-nd/4.0/>).

1. Introduction

The ever-increasing global demand for energy, coupled with the need to address the climate crisis and promote economic development, has spurred significant interest in the search for new renewable energy sources over the past few decades (Apergis and Payne, 2010). Since 2010, solar energy has become the third renewable energy source, behind hydropower and wind (Ritchie et al., 2022). Among solar technologies, non-concentrated photovoltaic (PV) solar panels are the most commonly used for generating electrical energy (IEA, 2014).

Improving the efficiency of PV systems has been a primary goal in recent years, with a wide range of approaches being explored. On the one hand, various strategies have been proposed to maximize light absorption, including the use of transparent contacts (Musztyfaga-Staszuk et al., 2022; Ahlswede et al., 2008), Silicon texturization (Abdullah et al., 2016; Müller-Meskamp et al., 2012), antireflective coatings (Sarkin et al., 2020; Shanmugam et al., 2020) or bifacial systems (Guerrero-Lemus et al., 2016; Sun et al., 2018), which are among the most promising. Bifacial solar cells (BSC) allow for light absorption through both the front (direct light) and rear (albedo) faces, resulting in up to 30% improvement in energy efficiency (Dullweber and Schmidt, 2016). With

production costs similar to those of monofacial cells (Guerrero-Lemus et al., 2016) bifacial cells are expected to capture 70% of the PV market share by 2030, compared with 20% in 2020, according to the international technology roadmap (Mouhib et al., 2022). The role of the albedo in the efficiency of the cell has been recently studied (Mekemeche and Beghdad, 2021; Raina and Sinha, 2021).

Although a lot of advances are being made in perovskite technology (Sharma et al., 2022), including optimizing light trapping in bifacial cells (Fan et al., 2022; Obratzsova et al., 2022), PERC technology has become the main options in the photovoltaic market due to its interesting cost and efficiency (Kim et al., 2022). A lot of research is being conducted recently in the improvement of the efficiency of these cells, for example to reduce recombination tailoring the passivation layer (Kim et al., 2022), rear contacts design and optimization for bifacial use (Chen et al., 2019; Tang et al., 2020; Dikshit et al., 2021), selective emitter design and optimization (Zhang et al., 2020; Dullweber et al., 2020; Wang and Chen, 2021). On the other hand, strategies have also been proposed to reduce the operating temperature of PV cells and improve their efficiency in recent years (Kumari et al., 2022; Sharaf et al., 2022), including airflow cooling methods (Valeh-E-Sheyda et al., 2014; Cuce and Cuce, 2014), photovoltaic-thermal collectors (PV/T) (Riffat and Cuce, 2011; Hu et al., 2021), water spraying (Krauter, 2004) or radiative cooling (Zhao et al., 2019) among others. This temperature reduction directly impacts the

* Corresponding author at: Dpto. Ing. Eléctrica, Electrónica y Comunicación, Universidad Pública de Navarra, 31006 Pamplona, Spain.

E-mail address: angel.andueza@unavarra.es (A. Andueza).

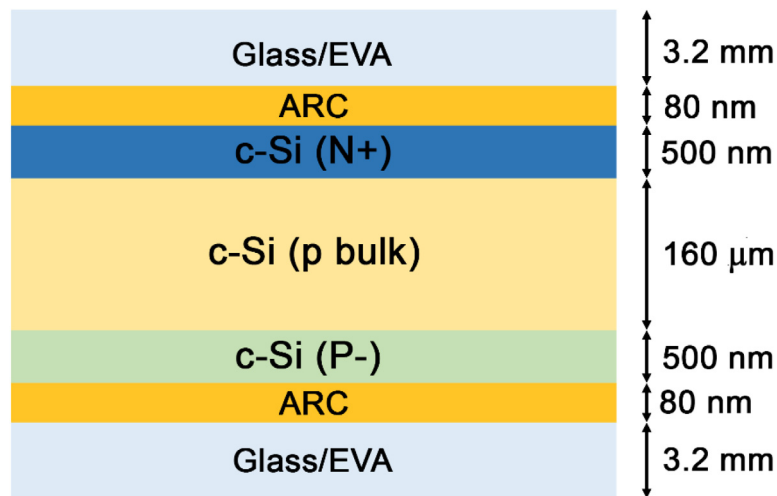


Fig. 1. Schematic cross-section of the simplest modeled PERC bifacial solar cell structure (the thickness of the layers is not drawn to scale).

cell efficiency as much as 0.4% per °C. Radiative cooling of photovoltaic modules has been extensively investigated recently, in single sided silicon cells (Ahmed et al., 2021; Zhan et al., 2023; Gao et al., 2022) and in bifacial cells (Hu et al., 2021; Zhou et al., 2022; Xia et al., 2023). The joint optimization of light trapping and radiative cooling has also been studied (Heo et al., 2022; Silva-Oelker and Jaramillo-Fernandez, 2022).

The purpose of this work is to go a step further studying the combined effect of light trapping and radiative cooling in bifacial PERC cells. To improve the both effects, we analyze different patterns for texturing the four surfaces of the panel: silicon and glass front and albedo sides. The main issue to address in this global optimization is the possible cross effects between the two sides of the bifacial panel. For example, if texturing increases the rear silicon surface to increase albedo absorption results in decreasing significantly the direct radiation, the net effect would be detrimental for solar cell efficiency.

There are three different spectral ranges relevant for the purpose of this work. First, to maximize photocurrent generated, a silicon cell has to absorb as much radiation as possible in the interval where it is converted in current, from 0.3 to 1.2 μm. Second, the emissivity of the cell must be maximized in the 8 to 13 μm interval, which corresponds to a nearly transparent region in the atmosphere and facilitates the radiative emission between the panel surface and outer space. Moreover, by attaining an emissivity close to 1 within the 16 to 25 μm range, the second window region can still be utilized despite its lower transmission characteristics. And third, there is an intermediate wavelength region from 1.2 to 5 μm where the sun still provides almost 164 W/m² but is useless for current production on silicon photovoltaic panels. The optical characteristics of the ideal panel would be (i) very low reflectivity in the visible range, (ii) very high one in the closer infrared (1.2 to 5 μm) and (iii) high emissivity in the thermal infrared window. In the rest of the paper we present computer calculations of different surface texturizations on PERC cell and the evaluation of the abovementioned desired characteristics. In the range of texturing patterns and sizes investigated, cross effects between sides are negligible. Besides, in general terms, silicon texturing increases light trapping and glass texturing enhances radiative cooling, but the thermal gain due to the closer infrared window cannot be avoided.

2. Materials and methods

In this section, we describe the materials and methods used to analyze light absorption and thermal radiation optimization on a

bifacial PERC solar cell. It is important to note that all the results presented are numerical calculations.

2.1. Bifacial solar cell used model

In order to perform the simulations, we begin by defining a precise model of a solar cell with all materials and dimensions well established. We have used the 3D electromagnetic model of the PERC bifacial solar cell (Boukourt and Hadri, 2019; Sugiura et al., 2020), as shown in Fig. 1, which is based on a standard low-doped crystalline Si (p bulk) 160 μm wafer. The top and rear surfaces of the silicon wafer have a 500 nm thick heavily doped n+ emitter and p+ back surface field (BSF) layer. The doping concentration of the bulk, the emitter, and the BSF layer were selected based on typical values (Riverola et al., 2018), with concentrations of 1×10^{19} , 3.3×10^{20} , and 1.5×10^{19} cm⁻³, respectively. An anti-reflective coating (ARC) layer of Silicon Nitride (Si₃N₄), conformal with the surface of silicon, is considered between the silicon and encapsulation layer. The thickness of the ARC layer is 80 nm, which corresponds to the λ/4 matching section to maximize the absorption of the silicon wafer around a wavelength of 550 nm. Finally, both sides of the solar cell encapsulate with around 3.2 mm ethylene-vinyl acetate (EVA) and soda-lime-low-iron glass. The front and back contact fingers are not included in the 3D model since the simulated wavelengths are significantly shorter than the usual distance between contacts on commercial cells, which is around 2 mm (Riverola et al., 2018).

2.2. Simulation tools

The absorptivity and emissivity of the bifacial PERC solar cell is calculated across the visible, near-infrared (NIR), and mid-infrared (MIR) ranges using two simulation tools: Grating Diffraction Calculator (GD-Calc) and CST MICROWAVE STUDIO™. Each one calculates the absorptivity and emissivity in a different wavelength region: GD-Calc for the visible, NIR, and short-wavelength MIR (from 0.3 to 8 μm), and CST for the long-wavelength MIR range from 8 μm to 25 μm.

GD-Calc is a software package developed by Kenneth C. Johnson and integrated into Matlab that uses rigorously coupled-wave analysis (RCWA) (Johnson, 2014, 2005). It is ideal for solar cell problems since it can simulate structures much larger than the shorter wavelength of the calculation. Note that the total thickness of the modeled PERC bifacial solar cell is around 6.6 mm, and the shortest wavelength simulated is 0.3 μm, differing by almost

four orders of magnitude. We selected a spatial resolution of the simulator to obtain accurate results and a reasonable simulation time for each wavelength. For the textured regions in glass and silicon, and considering the micrometric texturing sizes, the minimum spatial resolution selected was 10 nm, while the spectral resolution was 5 nm. Since GD-Calc assumes infinite spatial and temporal coherence, it predicts interference phenomena that are not real. To reduce the ripple noise introduced by this artifact, obtained data were filtered with a Savitzky–Golay smoothing method (with a polynomial degree of 8).

CST MICROWAVE STUDIO™ is a commercial software package that uses the Finite Integration time-domain Method (FIM) (Clemens and Weil, 2001) for electromagnetic field simulation in the microwave, terahertz, and optical range. We selected CST for its ability to provide highly accurate results within a short simulation time. In order to calculate the absorptivity of the bifacial solar cell from 8 to 25 μm , we used a frequency solver tool with tetrahedral adaptive mesh refinement. The textured glass unit cell has been modeled with an infinite thickness, assuming that all incident radiation is absorbed by the glass and not transmitted. This approach is consistent with the actual model, given that the thickness of the glass (3.2 mm) is much larger than the MIR wavelength range, which corresponds to atmospheric windows.

The simulations were based on refractive index data for the materials used, which were obtained from the scientific literature. Further information on the refractive index and albedo models used in the presented calculations can be found in the Supplementary Materials section (Urdirroz et al., 2023).

2.3. Power balance performance

To assess the thermal performance of a bifacial solar cell, we must calculate the radiative power balance of the system. Radiation emitted from the solar cell's surfaces escapes into space through Earth's atmosphere, while some is trapped by the surrounding atmosphere and contribute to the panel's thermal balance. During daylight hours, the solar cell's thermal power balance is significantly affected by the absorption of solar radiation in the 0.3 to 4 μm wavelength range. The final component of the radiative power balance is the absorbed non-radiative power from the surrounding environment, which primarily results from conductive and radiative thermal processes. Considering all of this, the thermal performance of the PERC bifacial solar cell is given by

$$P_{net} = P_r - P_a - P_{sun} - P_{nr} \quad (1)$$

where P_r is the radiated power from the cell, P_{sun} , and P_a are the absorbed irradiance by the cell from the sun and the atmosphere, respectively, and P_{nr} is the absorbed non-radiative power density from the surrounding. See more details in supplementary materials (Urdirroz et al., 2023).

To determine the increase in thermal efficiency achieved by texturing the surfaces, we define a parameter for the difference in net thermal power. This parameter is obtained by subtracting the thermal power balance of the textured PERC bifacial solar cell from that of the flat one. We consider that the environmental conditions, the radiator thermal insulation, and wind speed for both samples are identical. Hence, the conduction and convection thermal process undergone by both bifacial solar cells is equal, and the non-radiative absorption terms cancel each other in the differential power balance. Considering this, Eq. (1) expresses as follows:

$$P_{diff} = P_{net}^t - P_{net}^f = (P_r^t - P_r^f) - (P_a^t - P_a^f) - (P_{sun}^t - P_{sun}^f) \quad (2)$$

$$= \Delta P_r - \Delta P_a - \Delta P_{sun}$$

where the superscripts t and f refer to textured and flat samples, respectively. A positive differential net thermal power balance parameter (P_{diff} , as shown in Eq. (2)) is necessary to achieve a reduction in temperature through radiative cooling. To increase the power radiated (ΔP_r), texturization must be implemented while ensuring that the absorbed power from the sun and atmosphere remains equal or reduced. Conversely, a negative P_{diff} indicates additional thermal power absorption, which can increase the temperature of the solar cell and counteract the benefits of texturing.

3. Results and discussion

In this section, we present the results obtained trying to tailor the panel interfaces to optimize their performance in three wavelength intervals with different purposes: (i) the visible range, minimum reflection and maximum absorption by both sides, (ii) near-infrared, minimum absorption by both sides and (iii) atmospheric infrared, maximum emissivity in the side facing the sky. For this purpose, we have set up a simulation procedure to provide the electromagnetic performance (reflection, emission, and absorption) in the presented PERC bifacial panel.

3.1. Optimization of light absorption in the visible range

Our primary objective is to optimize the surface texturing of the silicon layer to obtain the maximum generated photocurrent. According to its good performance observed in other studies (Mavrokefalos et al., 2012; Gaucher et al., 2016; Cheng et al., 2012; Huang et al., 2019), we have decided to use a texture of close-packed inverted pyramids with a period and height of 2 and 1.41 μm , respectively. Note that the angle of the inverted pyramids, 54.7°, is determined by the crystal structure of silicon (111) in microfabrication using lithography and etching (Prakash et al., 2013). We have studied the mutual influence of texturing on the front and rear sides by simulating the silicon layer illuminated from both sides. We have considered four cases, summarized in Fig. 2: (a) a flat silicon wafer without texturing, (b) a silicon wafer with textured top surface and flat rear side, illuminated from the front, (c) a silicon wafer with a flat front side and textured rear side, illuminated from the rear side, and (d) a silicon wafer with texturing on both sides, with illuminated from one of them. We refer to direct incidence when the light strikes the front side and albedo incidence when it reaches the rear side.

Fig. 3 depicts the absorption spectra of a silicon wafer with and without texturing under direct (Fig. 2(b)) and albedo (Fig. 2(c)) light incidence. Albedo's absorptivity has been calculated as average absorption spectra on the rear side from Lambert's cosine law, where the absorption spectrum for an incidence angle is weighted by its incidence angle. Hence, the average absorption can be calculated as,

$$\overline{A_{c-si}}(\lambda, \theta) = \sum_{\theta=0}^n A_{c-si}(\lambda, \theta) \cdot \cos\theta \quad (3)$$

where θ is the incidence angle of the albedo and $A_{c-si}(\lambda, \theta)$ is the calculated absorptivity spectrum for an angle θ . The incidence angle of the albedo was swept from 0° to 70°, with a step of 10°. The presented results show that significant absorption enhancement is achieved when one of the silicon faces is textured. Specifically, the inverted pyramid pattern raises the absorptivity and average absorptivity values over the visible range for direct and albedo incidence by 17.8% and 3.8%, respectively, compared to the flat one.

Now, we examine the cross-influence when both sides are textured (Fig. 2(d)). We start by considering an unchanged front-side texture under direct incident but modifying the rear texturing.

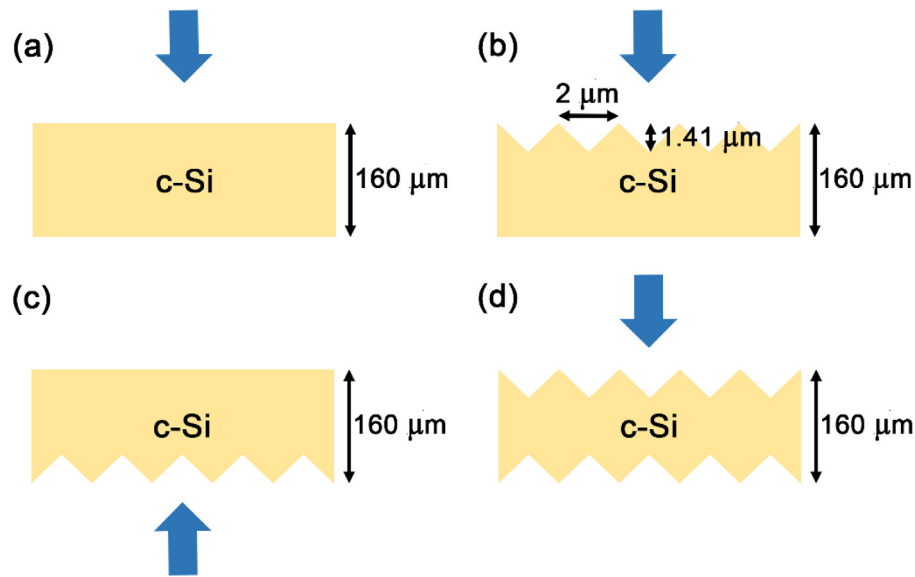


Fig. 2. Schematic of simulated silicon wafers: (a) flat surfaces, (b) Square inverted pyramid texturing on the front side, (c) Square inverted pyramid texturing on the rear side, (d) Square inverted pyramid texturing on both sides. The height and period of the texture are labeled in (b) and are the same all cases. The blue arrow represents the incident light direction.. (For interpretation of the references to color in this figure legend, the reader is referred to the web version of this article.)

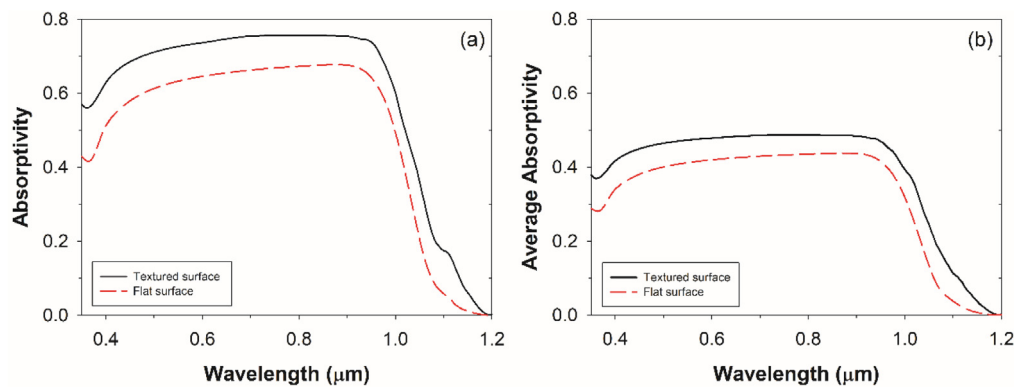


Fig. 3. Absorption spectra on (a) direct and (b) albedo incidence for a silicon wafer textured with inverted pyramids (solid black line) and a flat silicon wafer (red dashed line). The pitch and height of the inverted pyramids are 1.41 a 2, respectively.. (For interpretation of the references to color in this figure legend, the reader is referred to the web version of this article.)

The front-side texturing is based on inverted pyramids with a pitch of $2 \mu\text{m}$, while the rear one sweeps from a flat surface to four inverted pyramid patterns with a height of $1.41 \mu\text{m}$ and a period varying from 1 to $4 \mu\text{m}$. The spectra shown in Fig. 4 indicate that the absorption in the visible range for direct incidence does not change significantly when the texturing on the rear side is modified. The differences in the absorption spectra arise from minor variations in the near-IR absorption response between 1 and $1.2 \mu\text{m}$ having an average absorptivity of both structures from 0.3 to $1.2 \mu\text{m}$ around 0.76 in all cases, with an error lower than 1% . Therefore, the absorption of the silicon layer can be considered independent of the rear-face texturing under direct incidence. Consequently, texturing optimization on the rear face should only focus on enhancing albedo absorption. This finding aligns with previous studies conducted on bifacial systems (Frank et al., 2012).

Next, we analyze the contribution of albedo by using the previous silicon texturing patterns on both faces with the light now incident on the rear side (Fig. 2(d)). Fig. 5 shows the average absorption for each texturing pattern. As can be seen, texturing enhances the absorption on the rear face in all cases. The average absorptivity increases by almost 15% in the best case (pitch of

$1 \mu\text{m}$). Besides, the difference between average absorptivity is always lower than 4% as the period of textures varies. According to the obtained results, we can conclude that the optimization of silicon absorption by texturing can be designed independently for the light incidence on the front side, as no significant cross differences in improvement were observed. From previous results, we calculate a current density of 40.85 mA/cm^2 for direct incidence when silicon is textured on both sides (more details of these calculations are shown in the Supplementary materials (Urdirroz et al., 2023)). The current density due to albedo depends on the ground material, with three typical substrates considered in solar cell applications: green grass (6.7 mA/cm^2), sand (18.4 mA/cm^2), and concrete (8.9 mA/cm^2). Therefore, the maximum current generated for the simulated bifacial textured cell reaches the value of 59.25 mA/cm^2 for the best case.

3.2. Mid range radiative cooling optimization

Solar panels under sun radiation reach operating temperatures above the ambient value. However, the conversion efficiency of a solar cell decreases as temperature rises, between 0.35 and $0.4\%/^\circ\text{C}$ (Solar and Solar, 2022). Also, their durability suffers at

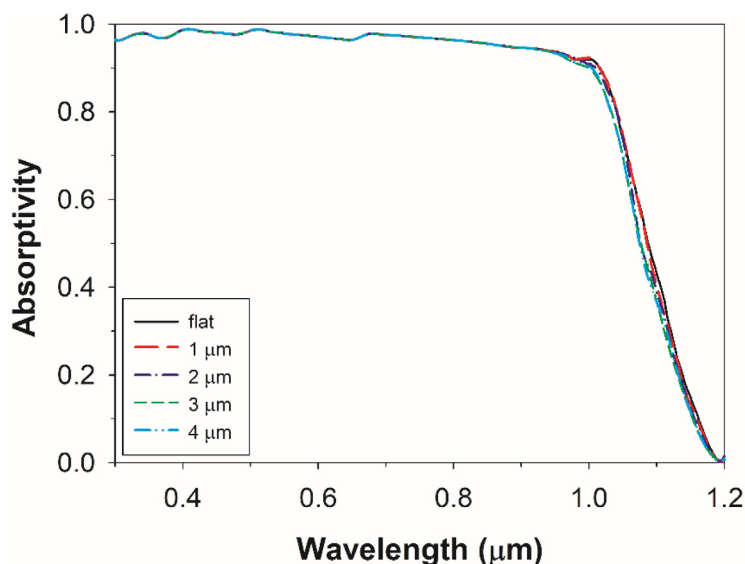


Fig. 4. Absorptivity of a 160 μm thickness silicon layer textured on the front side by inverted pyramids of pitch 2 μm, height 1.41 μm and varying the texturing of the rear one. The inverted pyramids on the rear side have the same height, 1.41 μm, and vary the pitch. The calculations were performed considering direct light incidence.

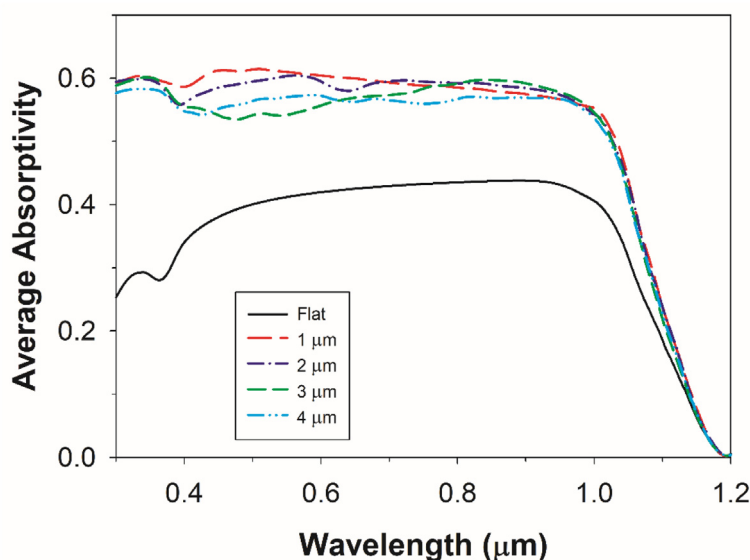


Fig. 5. Albedo’s average absorptivity for a doubly textured silicon layer where the front side has inverted pyramids texturing of pitch 2 μm and height 1.41 μm, and the rear side is modified.

higher temperatures. To reduce panel temperature, the maximization of radiative cooling is a promising strategy (Andueza et al., 2021; Zhu et al., 2015). As this process occurs in the wavelengths of the atmospheric window (8–13 μm), its maximization requires the highest possible emissivity of the solar cell for these wavelengths. We propose to obtain it by texturing the encapsulating glass layer.

As has been explained, and according to Eq. (1), a radiator will only generate effective cooling when the output power exceeds the total absorbed one, resulting in a positive net cooling power. Ideally, the energy absorbed from the sun should be minimum in the 1.2 to 5 μm region, while the energy emitted in the transparent window spectrum should be maximum. In this study, we evaluated the thermal net power balance of the designed bifacial panel by introducing a glass texturing of square pyramids with height and pitch of 10 and 2 μm, respectively. Fig. 6 presents the calculated emissivity compared with the flat glass one. The

texturing of the glass was selected based on the performance exhibited by square pyramids on the glass, as previously demonstrated (Andueza et al., 2021). As shown in Fig. 6, the emissivity for the textured glass is close to 1 in the considered range, similar to an ideal blackbody. The average emissivity through the atmospheric window (the integral of the absorptivity spectrum in the wavelength range 8–13 μm) for flat and textured glass is 0.87 and 1, respectively. Besides, a pyramid-textured glass does not present incidence directional emissivity changes in this range, which also helps to maximize the radiated power P_r (Andueza et al., 2021). Therefore, the pyramid texturing pattern on glass performs significantly better than the flat one and may help reduce the thermal absorption of the system.

In the thermal power balance calculations, two ranges are considered: from 0.3 to 5 μm, dominated by the absorbed solar power (P_{sun}), and from 5 to 25 μm, dominated by the glass radiated power (P_r). A fundamental factor in these calculations is the

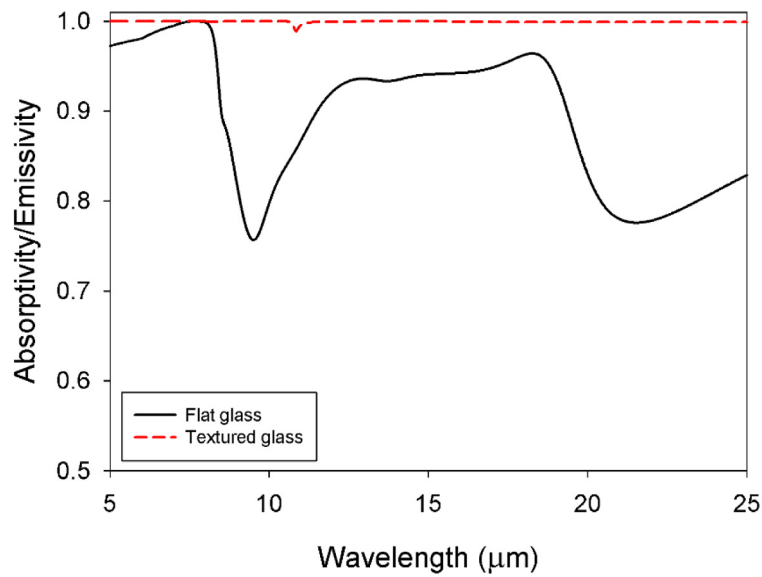


Fig. 6. Emissivity spectra of a flat glass sample (solid black line) and textured glass with pyramids (dashed red line). The calculations were carried out at normal incidence with infinite glass thickness.. (For interpretation of the references to color in this figure legend, the reader is referred to the web version of this article.)

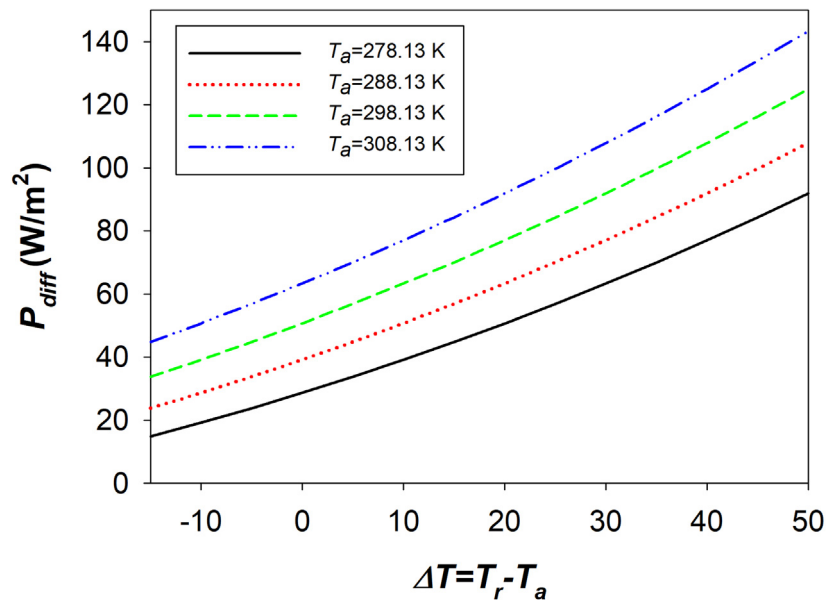


Fig. 7. Differential net cooling power (P_{diff}) from 5 to 25 μm as a function of temperature difference. The ambient temperature of each curve is indicated in the figure.

temperature difference (ΔT) between the ambient temperature (T_a) and the radiator temperature (T_r). Non-radiative power does not depend on the emissivity and its contribution cancels in Eq. (2). Fig. 7 shows the net power balance (P_{diff}) as a differential value between the net cooling power of the textured glass and the flat one. To demonstrate the effect of texturing on the power balance in the mid-infrared (MIR) range, we considered four typical ambient temperatures in a mid-latitude zone like Spain. In the case of solar cells, assuming the Nominal Maximum Operation Temperature (NMOT) of 60 °C, the differential temperature (ΔT) is between 20 and 35 °C under T_a . The best cooling performance at low ambient temperatures ($T_a = 278.13$ K) is 70 W/m². As T_a increases, despite the reduction in ΔT , the cooling capacity increases to around 100 W/m². Based on these results, it is possible to obtain an extra net cooling power, between 70 and 100 W/m², under daytime conditions by texturing the glass layers with the considered pyramids.

3.3. Combination of light-trapping and radiative cooling strategies in a perovskite bifacial solar cell

To complete the performance analysis, we now consider a PERC bifacial solar panel and calculate the absorptivity of the silicon considering all possible combinations of surface texturing. Several bifacial cells with different textured structures on silicon were analyzed. The results (see Supplementary material section (Urdirroz et al., 2023)) showed that inverted pyramids was the best structure in terms of light trapping performance and was selected for the final panel design. Fig. 8 shows a cross-section of the PERC bifacial solar cells simulated: (a) all flat, (b) glass-textured with flat silicon, (c) flat glass with textured silicon, and (d) doubly textured bifacial panels (glass and silicon). Correspondingly, Fig. 9 presents the calculated absorptivity spectra for the exposed samples.

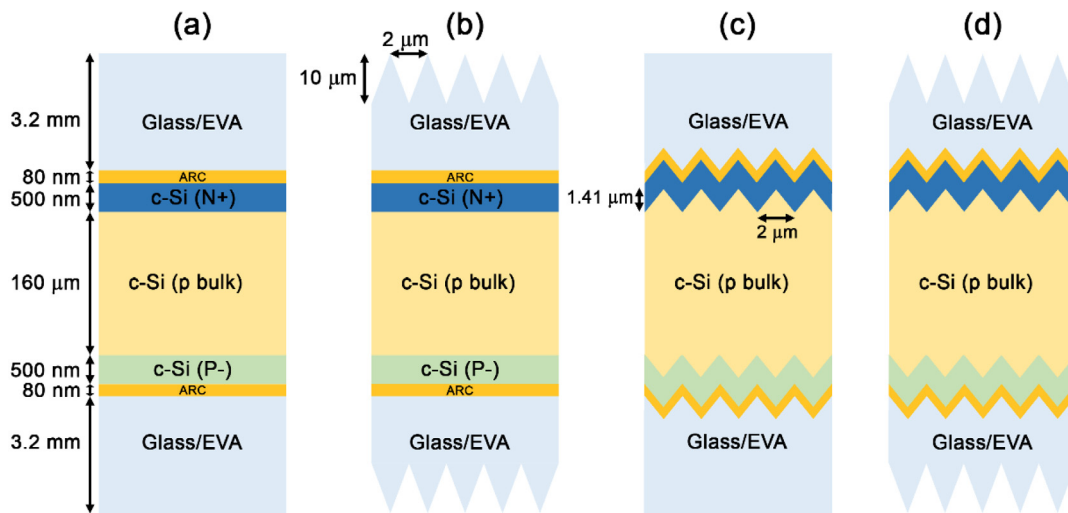


Fig. 8. Cross-section schematic of the modeled encapsulated PERC bifacial solar cells NPP structure (the thickness of the layers has not been drawn to scale): (a) flat, (b) glass-textured but flat silicon, (c) Si-textured but flat glass, and (d) doubly textured.

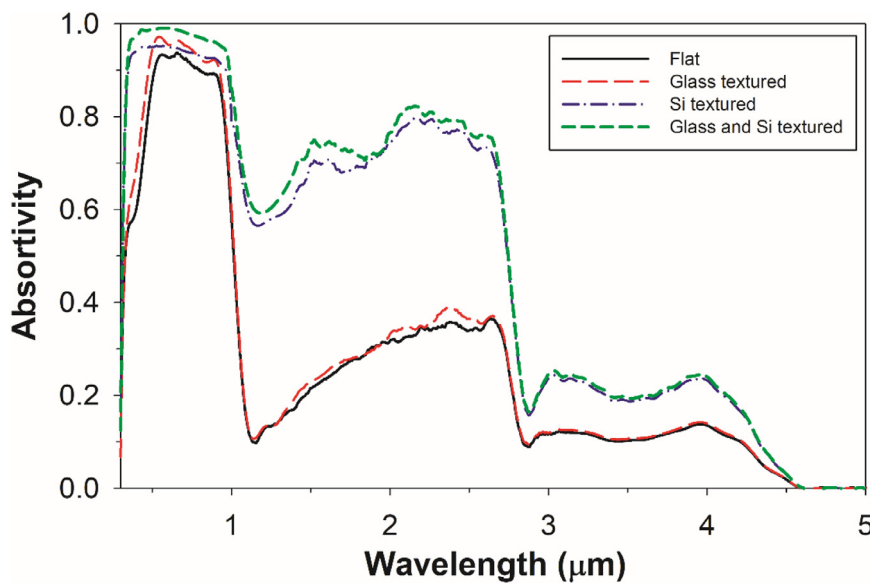


Fig. 9. Dependence of the silicon absorptivity on the BSC textures. (solid black line) flat BSC without textures, (dashed-red line) flat BSC with glass texturing, (dot-dashed blue line) silicon textured BSC, and (short-dashed green line) BSC with glass and silicon texturing. The results presented correspond to the normal incidence in all cases.. (For interpretation of the references to color in this figure legend, the reader is referred to the web version of this article.)

The PERC panels with flat silicon exhibit significantly lower absorptivity regarding textured samples. The silicon texturing aimed to enhance light trapping, and this effect is not limited to visible light but extends to the NIR range from (1.2 to 4 μm), where the increase is proportionally more significant. Glass texturing, on top of the silicon surface, offers an additional enhancement in visible absorptivity but not in NIR zone. In contrast, the absorptivity of the textured silicon panels is higher and more consistent along the spectra.

Next, we can compare the performance of each proposed PERC panel. Three different parameters need to be assessed: (i) the current gain, (ii) the sun heating power gained from (0.3 to 5 μm), and (iii) MIR radiative cooling from (5 to 25 μm). Therefore, we calculate three figures of merit normalized to a flat bifacial PERC panel. The first one is the normalized enhancement of total current density from 0.3 to 1.2 μm (direct and albedo), calculated as $\Delta J = (J_t - J_f)/J_t$. To calculate the albedo's current density, we consider a ground of sand. The second one is the thermal power balance from 0.3 to 5 μm in direct incidence, calculated

as $\Delta P_{th} = P_{tht} - P_{thf}$. Finally, the third one is the differential net thermal power balance from 5 to 25 μm (ΔP_{diff}) with a T_r and T_a of 333 K (corresponding to a 60 °C operating temperature) and 298 K, respectively. The subscripts t and f refer to textured and flat samples, respectively. The results are presented in Table 1, where J_f and P_{thf} are 49.7 mA/cm² and 553 W, respectively. Note that the current density and the thermal power balance values indicate inside the parentheses. The net power balance calculations for each analyzed structure can be found in the supplementary material section (Urdirroz et al., 2023).

Considering the current density generated, the textured silicon and glass surfaces consistently outperformed their flat counterparts. As is seen in Fig. 8 (from left to right), the doubly textured structure (d) yielded the highest photocurrent gain of 15.3%. A similar trend was observed for the heat gain due to near-infrared solar radiation, which increased from 24 W to 179 W relative to the flat structure. Only the textured glass structures (b and d) generated a radiative cooling power of 95 W. While all textured surfaces produced larger photocurrents, the thermal effects were

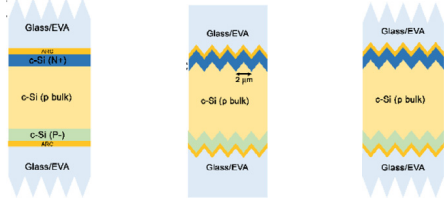
Table 1

Summary of the current density, infrared thermal power gains, and net power balance in the MIR range for the textured PERC samples studied.

Sample\Figure of merit	ΔJ (%)	ΔP_{th} (W)	ΔP_{diff} (W)
(b) Glass Textured flat-silicon BSC	4.4% (52.0 mA/cm ²)	−24 W (577 W)	95 W
(c) Flat-glass textured-silicon BSC	9.5% (55.0 mA/cm ²)	−192 W (745 W)	0 W
(d) Totally-textured BSC	15.3% (58.8 mA/cm ²)	−179 W (732 W)	95 W

Table 2

Summary of current density and net thermal power (from 0.3 to 25 μm) gains weighted by the flat PERC panel.



Current Gain	4.4%	9.5%	15.3%
Thermal Gain	12.8%	−34.7%	−15.2%

not as clear. The heating caused by the near-infrared radiation was not offset by the cooling through the atmospheric window, resulting in a net power increase for all structures. To simplify the comparison of the panels, we present Table 2, which shows the combined thermal power of the entire spectrum and the current density changes as a percentage of the flat structure.

Only the flat silicon with textured glass offers a net power gain in both parameters, albeit a smaller one in photocurrent. On the other hand, the case of both textured materials, silicon, and glass, results in the maximum current density gain with a moderate thermal power loss.

To obtain a definitive assessment of panel efficiency for different structures, photonic and thermal effects must evaluate together. A relevant parameter is the cell efficiency degradation with temperature, which lies in the interval of 0.35–0.4% per degree Celsius. However, calculating the panel temperature requires a thermal model of the panel, which is outside the scope of this paper. Moreover, the results are dependent on atmospheric conditions and panel installation details. Therefore, we do not convert the thermal power (in watts per square meter) into actual temperature. Instead, we present two figures of merit, as shown in Table 2, which should combine for specific applications.

Moreover, the effect of the rear face of the bifacial panel is strongly dependent on the detailed characteristics of its panel installation, particularly on the reflectivity of the environment facing the back of the solar cell. The results presented in this section have been calculated for direct incidence, considering the solar power on the front side of the BSC. As previously shown, albedo incidence can generate extra current density up to 30% of the direct incidence. Besides, the ground's temperature, typically close to the ambient temperature, limits the radiated power of the glass by the rear side. Therefore, reliable figures of merit for the back face require many assumptions.

4. Conclusions

In this work, we have investigated the performance of bifacial solar panels with passivated emitter and rear cell (PERC) architecture under various configurations of the silicon surface (solar cell) and glass surface (encapsulation). We aimed to enhance light trapping and radiative cooling through computer simulations of different panel structures.

Our first significant result was that both faces of the panel have an independent performance since their cross-effects are

negligible. Therefore, we can consider the four surfaces of the bifacial solar panel separately: the upper and lower sides of the silicon layer will determine the photon absorption (direct and albedo), while the glass layers will define the radiative cooling behavior.

Qualitatively we can conclude that silicon texturing significantly enhances light trapping. But this happens for all the spectrum, including the thermal power absorbed from the sun's near-infrared emission. On the other hand, encapsulating glass texturing increases the radiative cooling of the panel independently of the silicon surface. Considering both effects simultaneously, the thermal gain from the sun's near-infrared emission is greater than the radiated power in the atmospheric window, leading to higher temperatures.

In order to provide a quantitative assessment of the effects of the different surface configurations, we calculated figures of merit. From these values, we can conclude that:

- Texturing both surfaces (silicon and glass) results in a 15% increase in photocurrent and thermal power compared to a flat surface panel.
- The rear side of the panel can provide up to 30% extra current, but its thermal effect is highly dependent on installation details and atmospheric conditions.

The surface texturing strategies we studied are insufficient to achieve optimal light trapping and radiative cooling simultaneously. To achieve better thermal behavior while maintaining visible light absorption, a surface that changes from maximum absorption in the visible spectrum to maximum reflectance in the near-infrared is necessary. However, such a surface would require more sophisticated and likely expensive alternatives, such as metasurfaces.

Declaration of competing interest

The authors declare the following financial interests/personal relationships which may be considered as potential competing interests: Joaquin Sevilla Moroder reports financial support was provided by Departamento de Desarrollo Económico via Project DESAFIO (Desarrollo de estructuras fotónicas para aplicaciones fotovoltaicas).

Data availability

Data will be made available on request.

Acknowledgments

This work has been partially supported from Departamento de Desarrollo Económico of Navarra, Spain via Project DESAFIO, Desarrollo de eStructurAs FotónIcas para aplicaciones fOtovoltaicas.

Appendix A. Supplementary data

Supplementary material related to this article can be found online at <https://doi.org/10.1016/j.egy.2023.07.047>.

References

- Abdullah, M.F., Alghoul, M.A., Naser, H., Asim, N., Ahmadi, S., Yatim, B., Sopian, K., 2016. Research and development efforts on texturization to reduce the optical losses at front surface of silicon solar cell. *Renew. Sustain. Energy Rev.* 66, 380–398. <http://dx.doi.org/10.1016/j.rser.2016.07.065>.
- Ahlsvede, E., Mühleisen, W., Bin Moh Wah, M.W., Hanisch, J., Powalla, M., 2008. Highly efficient organic solar cells with printable low-cost transparent contacts. *Appl. Phys. Lett.* 92, 2012–2015. <http://dx.doi.org/10.1063/1.2907564>.
- Ahmed, S., Li, Z., Javed, M.S., Ma, T., 2021. A review on the integration of radiative cooling and solar energy harvesting. *Mater. Today Energy*. 21, 100776. <http://dx.doi.org/10.1016/j.mtener.2021.100776>.
- Andueza, Á., Pinto, C., Navajas, D., Sevilla, J., 2021. Enhanced thermal performance of photovoltaic panels based on glass surface texturization. *Opt. Mater. (Amst)* 121, <http://dx.doi.org/10.1016/j.optmat.2021.111511>.
- Apergis, N., Payne, J.E., 2010. Renewable energy consumption and economic growth: Evidence from a panel of OECD countries. *Energy Policy* 38, 656–660. <http://dx.doi.org/10.1016/j.enpol.2009.09.002>.
- Boukourt, N., Hadri, B., 2019. Bifacial n-PERC solar cell characterization. *Indian J. Phys.* 93, 33–39. <http://dx.doi.org/10.1007/s12648-018-1274-5>.
- Chen, W., Liu, R., Zeng, Q., Zhou, L., 2019. Low cost multicrystalline bifacial PERC solar cells – Fabrication and thermal improvement. *Sol. Energy* 184, 508–514. <http://dx.doi.org/10.1016/j.solener.2019.04.033>.
- Cheng, H.H., Chang, Y.Y., Chu, J.Y., Lin, D.Z., Chen, Y.P., Li, J.H., 2012. Light trapping enhancements of inverted pyramidal structures with the tips for silicon solar cells. *Appl. Phys. Lett.* 101, <http://dx.doi.org/10.1063/1.4755758>.
- Clemens, M., Weil, T., 2001. Discrete electromagnetism with the finite integration technique. *Prog. Electromagn. Res.* 32, 65–87. <http://dx.doi.org/10.2528/PIER00080103>.
- Cuce, E., Cuce, P.M., 2014. Improving thermodynamic performance parameters of silicon photovoltaic cells via air cooling. *Int. J. Ambient Energy* 35, 193–199. <http://dx.doi.org/10.1080/01430750.2013.793481>.
- Dikshit, A.K., Banerjee, P., Mukherjee, N., Chakrabarti, P., 2021. Theoretical optimization of double dielectric back reflector layer for thin c-Si based advanced solar cells with notable enhancement in MAPD. *Superlattices Microstruct.* 149, 106747. <http://dx.doi.org/10.1016/j.spmi.2020.106747>.
- Dullweber, T., Schmidt, J., 2016. Industrial silicon solar cells applying the passivated emitter and rear cell (PERC) concept—A review. *IEEE J. Photovoltaics*, 6, 1366–1381. <http://dx.doi.org/10.1109/JPHOTOV.2016.2571627>.
- Dullweber, T., Stöhr, M., Kruse, C., Haase, F., Rudolph, M., Beier, B., Jäger, P., Mertens, V., Peibst, R., Brendel, R., 2020. Evolutionary PERC+ solar cell efficiency projection towards 24% evaluating shadow-mask-deposited poly-Si fingers below the Ag front contact as next improvement step. *Sol. Energy Mater. Sol. Cells*. 212, 110586. <http://dx.doi.org/10.1016/j.solmat.2020.110586>.
- Fan, L., Lü, W., Hu, W., Han, D., Yang, S., Wang, D., Mai, Z., Wang, F., Liu, H., Yang, J., Yang, L., 2022. Enhanced photovoltaic output of bifacial perovskite solar cells via tailoring photoelectric balance in rear window layers with 1T-WS₂ nanosheet engineering. *Mater. Chem. Front.* 6, 2061–2071. <http://dx.doi.org/10.1039/D2QM00366j>.
- Frank, J., Rüdiger, M., Fischer, S., Goldschmidt, J.C., Hermlle, M., 2012. Optical simulation of bifacial solar cells. *Energy Procedia*. 27, 300–305. <http://dx.doi.org/10.1016/j.egypro.2012.07.067>.
- Gao, K., Shen, H., Liu, Y., Zhao, Q., Li, Y., Liu, J., 2022. Random inverted pyramid textured polydimethylsiloxane radiative cooling emitter for the heat dissipation of silicon solar cells. *Sol. Energy* 236, 703–711. <http://dx.doi.org/10.1016/j.solener.2022.03.040>.
- Gaucher, A., Cattoni, A., Dupuis, C., Chen, W., Cariou, R., Foldyna, M., Lalouat, L., Drouard, E., Seassal, C., RocaCabarrocas, P., Collin, S., 2016. Ultrathin epitaxial silicon solar cells with inverted nanopyramid arrays for efficient light trapping. *Nano Lett.* 16, 5358–5364. <http://dx.doi.org/10.1021/acs.nanolett.6b01240>.
- Guerrero-Lemus, R., Vega, R., Kim, T., Kimm, A., Shephard, L.E., 2016. Bifacial solar photovoltaics – A technology review. *Renew. Sustain. Energy Rev.* 60, 1533–1549. <http://dx.doi.org/10.1016/j.rser.2016.03.041>.
- Heo, S., Kim, D.H., Song, Y.M., Lee, G.J., 2022. Determining the effectiveness of radiative cooler-integrated solar cells. *Adv. Energy Mater.* 12, 2103258. <http://dx.doi.org/10.1002/aenm.202103258>.
- Hu, M., Zhao, B., Ao, X., Suhendri, Cao, J., Wang, Q., Riffat, S., Su, Y., Pei, G., 2021. Performance analysis of a novel bifacial solar photothermic and radiative cooling module. *Energy Convers. Manag.* 236, 114057. <http://dx.doi.org/10.1016/j.enconman.2021.114057>.
- Huang, Z.G., Gao, K., Wang, X.G., Xu, C., Song, X.M., Shi, L.X., Zhang, Y., Hoex, B., Shen, W.Z., 2019. Large-area MACE Si nano-inverted-pyramids for PERC solar cell application. *Sol. Energy*. 188, 300–304. <http://dx.doi.org/10.1016/j.solener.2019.06.015>.
- IEA, 2014. Technology Roadmap: Solar Photovoltaic Energy 2014 Edition. Int. Energy Agency, http://dx.doi.org/10.1007/SpringerReference_7300.
- Johnson, Kenneth C., 2005. GD-Calc. <https://kjinnovation.com/>.
- Johnson, K.C., 2014. Projection operator method for bi-periodic diffraction gratings with anisotropic/bianisotropic generalizations. *J. Opt. Soc. Am. A*. 31, 1698. <http://dx.doi.org/10.1364/JOSAA.31.001698>.
- Kim, J., Lee, S., Chowdhury, S., Yi, J., 2022. A brief review of passivation materials and process for high efficiency perovskite solar cell. *Trans. Electr. Electron. Mater.* 23, 1–5. <http://dx.doi.org/10.1007/s42341-021-00366-5>.
- Krauter, S., 2004. Increased electrical yield via water flow over the front of photovoltaic panels. *Sol. Energy Mater. Sol. Cells* 82, 131–137. <http://dx.doi.org/10.1016/j.solmat.2004.01.011>.
- Kumari, S., Pandit, A., Bhende, A., Rayalu, S., 2022. Thermal management of solar panels for overall efficiency enhancement using different cooling techniques. *Int. J. Environ. Res.* 16, 1–20. <http://dx.doi.org/10.1007/s41742-022-00431-8>.
- Mavrokefalos, A., Han, S.E., Yerci, S., Branham, M.S., Chen, G., 2012. Efficient light trapping in inverted nanopyramid thin crystalline silicon membranes for solar cell applications. *Nano Lett.* 12, 2792–2796. <http://dx.doi.org/10.1021/nl2045777>.
- Mekemeche, A., Beghdad, M., 2021. Impact of the environmental effective albedo on the performance of PERC solar cells. *Silicon* 13, 3991–3998. <http://dx.doi.org/10.1007/s12633-020-00707-8>.
- Mouhib, E., Micheli, L., Almonacid, F.M., Fernández, E.F., 2022. Overview of the fundamentals and applications of bifacial photovoltaic technology: Agrivoltaics and aquavoltaics. *Energies* 15, <http://dx.doi.org/10.3390/en15238777>.
- Müller-Meskamp, L., Kim, Y.H., Roch, T., Hofmann, S., Scholz, R., Eckardt, S., Leo, K., Lasagni, A.F., 2012. Efficiency enhancement of organic solar cells by fabricating periodic surface textures using direct laser interference patterning. *Adv. Mater.* 24, 906–910. <http://dx.doi.org/10.1002/adma.201104331>.
- Muszyfaga-Staszuk, M., Czupryński, A., Radev, R., 2022. Review of the chosen methods of producing front contacts to transparent conductive oxides layers in photovoltaic structures. *Energies* 15, 1–14. <http://dx.doi.org/10.3390/en15239026>.
- Obraztsova, A.A., Baretton, D., Furasova, A.D., Voroshilov, P.M., Auf der Maur, M., Orsini, A., Makarov, S.V., 2022. Light-trapping electrode for the efficiency enhancement of bifacial perovskite solar cells. *Nanomaterials* 12, 3210. <http://dx.doi.org/10.3390/nano12183210>.
- Prakash, A., Jency, J.G., Mathew, M.C., 2013. A review of various wet etching techniques used in micro fabrication for real estate consumption. *Int. J. Comput. Appl.* 975–8887.
- Raina, G., Sinha, S., 2021. A simulation study to evaluate and compare monofacial vs bifacial PERC PV cells and the effect of albedo on bifacial performance. *Mater. Today Proc.* 46, 5242–5247. <http://dx.doi.org/10.1016/j.matpr.2020.08.632>.
- Riffat, S.B., Cuce, E., 2011. A review on hybrid photovoltaic/thermal collectors and systems. *Int. J. Low-Carbon Technol.* 6, 212–241. <http://dx.doi.org/10.1093/ijlct/ctr016>.
- Ritchie, H., Roser, M., Rosado, P., 2022. Energy. <https://ourworldindata.org/energy>.
- Riverola, A., Mellor, A., Alonso Alvarez, D., Ferre Llin, L., Guarracino, I., Markides, C.N., Paul, D.J., Chemisana, D., Ekins-Daukes, N., 2018. Mid-infrared emissivity of crystalline silicon solar cells. *Sol. Energy Mater. Sol. Cells*. 174, 607–615. <http://dx.doi.org/10.1016/j.solmat.2017.10.002>.
- Sarkin, A.S., Ekren, N., Sağlam, Ş., 2020. A review of anti-reflection and self-cleaning coatings on photovoltaic panels. *Sol. Energy*. 199, 63–73. <http://dx.doi.org/10.1016/j.solener.2020.01.084>.
- Shanmugam, N., Pugazhendhi, R., Elavarasan, R.M., Kasiviswanathan, P., Das, N., 2020. Anti-reflective coating materials: A holistic review from PV perspective. *Energies* 13, 1–93. <http://dx.doi.org/10.3390/en13102631>.
- Sharaf, M., Yousef, M.S., Huzayyin, A.S., 2022. Review of cooling techniques used to enhance the efficiency of photovoltaic power systems. *Environ. Sci. Pollut. Res.* 29, 26131–26159. <http://dx.doi.org/10.1007/s11356-022-18719-9>.
- Sharma, R., Sharma, A., Agarwal, S., Dhaka, M.S., 2022. Stability and efficiency issues solutions and advancements in perovskite solar cells: a review. *Sol. Energy*. 244, 516–535. <http://dx.doi.org/10.1016/j.solener.2022.08.001>.
- Silva-Oelker, G., Jaramillo-Fernandez, J., 2022. Numerical study of sodalime and PDMS hemisphere photonic structures for radiative cooling of silicon solar cells. *Opt. Express* 30, 32965. <http://dx.doi.org/10.1364/oe.466335>.
- Solar, J., Solar, Jinko, 2022. Tiger Pro 72HC 525–545 W. www.jinkosolar.com (Accessed 19 April 2022).
- Sugiura, T., Matsumoto, S., Nakano, N., 2020. Bifacial PERC solar cell designs: Bulk and rear properties and illumination condition. *IEEE J. Photovoltaics*. 10, 1538–1544. <http://dx.doi.org/10.1109/JPHOTOV.2020.3013987>.
- Sun, X., Khan, M.R., Deline, C., Alam, M.A., 2018. Optimization and performance of bifacial solar modules: A global perspective. *Appl. Energy* 212, 1601–1610. <http://dx.doi.org/10.1016/j.apenergy.2017.12.041>.
- Tang, H.B., Ma, S., Lv, Y., Li, Z.P., Shen, W.Z., 2020. Optimization of rear surface roughness and metal grid design in industrial bifacial PERC solar cells. *Sol.*

- Energy Mater. Sol. Cells 216, 110712. <http://dx.doi.org/10.1016/j.SOLMAT.2020.110712>.
- Urdiruz, A., Itoiz, Unai, Sevilla, Iñigo, Andueza, Joaquín, 2023. Supplementary materials: Performance analysis of PERC bifacial silicon solar cells by combining radiative cooling and light trapping strategies based on surface texturing.
- Valeh-E-Sheyda, P., Rahimi, M., Parsamoghdam, A., Masahi, M.M., 2014. Using a wind-driven ventilator to enhance a photovoltaic cell power generation. Energy Build. 73, 115–119. <http://dx.doi.org/10.1016/j.enbuild.2013.12.052>.
- Wang, Z., Chen, F., 2021. Monitoring of monocrystalline silicon PERC solar cell with laser-doped selective emitter using infrared and electroluminescence imaging. Int. J. Electrochem. Sci. 16, 1–10. <http://dx.doi.org/10.20964/2021.09.11>.
- Xia, T., Chen, H., Wang, H., 2023. Self-protecting concave microstructures on glass surface for daytime radiative cooling in bifacial solar cells. Int. Commun. Heat Mass Transf. 142, 106666. <http://dx.doi.org/10.1016/j.ICHEATMASSTRANSFER.2023.106666>.
- Zhan, Y., Yin, H., Wang, J., Fan, C., 2023. Enhanced performance of diurnal radiative cooling for solar cells based on a grating-textured PDMS photonic structure. Mater. Today Commun. 35, 106117. <http://dx.doi.org/10.1016/j.MTCOMM.2023.106117>.
- Zhang, C., Shen, H., Sun, L., Yang, J., Wu, S., Lu, Z., 2020. Bifacial p-type PERC solar cell with efficiency over 22% using laser doped selective emitter. Energies 13, 1388. <http://dx.doi.org/10.3390/en13061388>.
- Zhao, D., Aili, A., Zhai, Y., Xu, S., Tan, G., Yin, X., Yang, R., 2019. Radiative sky cooling: Fundamental principles materials, and applications. Appl. Phys. Rev. 6, 021306. <http://dx.doi.org/10.1063/1.5087281>.
- Zhou, Y., Xia, T., Niu, X., Sun, S., Xu, L., Jian, Y., Wang, H., 2022. Enhancing radiative cooling performance for bifacial photovoltaic module using two kinds of polycarbonate films. J. Photonics Energy 12, 1–11. <http://dx.doi.org/10.1117/1.jpe.12.045501>.
- Zhu, L., Raman, A.P., Fan, S., 2015. Radiative cooling of solar absorbers using a visibly transparent photonic crystal thermal blackbody. Proc. Natl. Acad. Sci. USA 112, 12282. <http://dx.doi.org/10.1073/PNAS.1509453112>.